

Advancing Surface Plasmon Enhanced Fluorescence based POC technologies

Subjects: **Chemistry, Analytical | Optics | Green & Sustainable Science & Technology**

Contributor: Kalathur Mohan Ganesh , Seemesh Bhaskar , Vijay Sai Krishna Cheerala , Prajwal Battampara , Roopa Reddy , Sundaresan Chittor Neelakantan , Narendra Reddy , Sai Sathish Ramamurthy

Point-of-care (POC) diagnostic platforms are globally employed in modern smart technologies to detect events or changes in the analyte concentration and provide qualitative and quantitative information in biosensing. Surface plasmon-coupled emission (SPCE) technology has emerged as an effective POC diagnostic tool for developing robust biosensing frameworks. The simplicity, robustness and relevance of the technology has attracted researchers in physical, chemical and biological milieu on account of its unique attributes such as high specificity, sensitivity, low background noise, highly polarized, sharply directional, excellent spectral resolution capabilities.

photronics

plasmonics

fluorescence

nano-optics

nanomaterials

Materials science

Biosensing

Diagnostics

Thin films

sustainable engineering

1. Introduction

Different technologies are being continuously developed for achieving the successful and reliable diagnostics of human, biological and environmental health. With the advent of luminescence (fluorescence, phosphorescence, chemiluminescence) spectroscopy, numerous biosensing applications have evolved by leveraging the expertise of physicists, chemists, biologists and material scientists [1][2][3]. To further boost the performance of fluorescence-based biosensing technologies, plasmonic nanoparticles (NPs), nanohybrids and their nanocomposites with dielectric nanomaterials are extensively researched [4][5][6]. The utilization of plasmonic nanomaterials to augment the signal intensity from weakly fluorescent biomolecules and monitoring the shifts in the plasmonic resonant modes induced by several physico-chemical interactions in nano-dimensions and single-molecular limits has been explored [7][8][9][10][11]. The ability of the plasmonic nanomaterials to generate high-field intensity in their vicinity has attracted researchers from different fields [12][13][14][15][16][17][18][19]. In this regard, different shape, sizes, morphology, topography and geometrical architecture (core-shell, decorated, alloy) are explored to integrate their utility in nanophotonics, metasurfaces and miniaturized optoelectronic devices [20][21][22][23]. The excitation and emission intensities of the radiating dipoles are dramatically influenced by the high electric field profile of the plasmonic NPs, thereby resulting in significant changes in the overall quantum yield and lifetime [24][25][26]. The metal-fluorophore system effectively constitutes a resonant hybrid termed 'plasmophore' (plasmon + fluorophore) because emitted photons from the radiating dipoles trigger newer charge density perturbation pathways to generate plasmons that finally radiate into the far-field, carrying the attributes of both the metal and the fluorophore species [4][24]. In the process, the newer channels of radiative decay rate are realized with high photostability and dwindled lifetime [27].

[28][29]. This field of research has evolved into metal-enhanced fluorescence (MEF) where the conventional limitations of low sensitivity in fluorescence spectrophotometry are circumvented. A plethora of hybrid systems made up of plasmonic metal NPs and fluorescence molecules are employed based on the application of interest [30][31][32][33][34][35]. Such MEF systems are utilized for applications concerning forensics, immunoassays, single molecule detection, spectro-plasmonics and food and drug analysis, to name a few.

2. Effect of Pristine AuNPs in SPCE

Different methodologies have been adopted to interface the plasmonic materials with the light emitting radiating dipoles. The process of electrostatic adsorption is a chemical process where the surface of interest is functionalized with specific chemical agents so that the desired material of interest can be electrostatically adsorbed on the surface. These methods are highly reliable as they generally give great coverage of adsorbed molecules over the plasmonic interfaces due to electrostatic interaction. However, the method of electrostatic adsorption is time-intensive and demands the development of specific surface functionalization methodologies. On the other hand, the key highlight of the spin coating method is the time-effective approach where it enables the researcher to fabricate surfaces of interest with less time. However, the demerit of using the spin coating method is the need for a clear understanding of the interaction between the radiating dipoles, polymer and the plasmonic nanomaterials. The addition of these samples to one another can be modulated to obtain the desired outcome. For instance, the direct addition of the nanomaterial to the polymer solution and further addition of the fluorescence dye solution would result in a variable fluorescence enhancement depending on the concentrations of the polymer used. If higher concentrations are used, then the plasmonic NPs can become encapsulated with a polymer layer, generating a spacer layer between the subsequently added dye solution and the nanomaterials. Hence, it is of paramount importance to consider the aspects of polymer concentration and spin coating parameters very carefully to realize effective fluorescence enhancements. Additionally, the need for the use of specific polymer solution in the case of the spin coating method is another drawback as compared to the electrostatic adsorption, as there is no need for the incorporation of polymer in the latter method.

By introducing AuNPs of different architectures on a gold substrate through electrostatic adsorption and spin-coating methods, multiple coupling structures for the SPCE system were facilitated, leading to 40- and 55-fold enhancements compared to free space (FS) emission, respectively. The diverse enhancement effect is due to novel “hot-spot” plasmonic structures, an intense EM field within the system, plasmonic properties and the process of coupling. Spin-coating based deposition of AuNPs can be used to easily build new enhancing systems with high efficiency without complex modifications, whereas the electrostatic adsorption of AuNPs provides a uniform modification, establishing highly sensitive and stable platform, which can broaden the application of SPCE in both fluorescence-based sensing and imaging.

LSPR occurs due to the energy transfer from the excited light to the collective oscillation of free electrons around the NPs, leading to a strong absorption of optical energy. The absorption peak depends on the size, shape, aggregation state, and dielectric environment. Nanoscale contacts between metal structures to form nanogap junctions are crucial plasmonic geometries. Hence, the close junctions between metallic NPs and continuous films

are effective plasmon modulation systems that can induce intense interactions between localized and propagating surface plasmons to generate “hot-spots” along with enormous enhancement of the EM field under certain conditions. This phenomenon can be used to build new plasmon-based enhanced systems like SPR which has been increasingly applied in sensing and clinical detection because of its sensitivity to refractive index variations, label-free detection, and real-time monitoring [36].

3. Effect of Au-Decorated SiO_2 (AuSil), Metal–Dielectric Nanohybrids in SPCE

There has been extensive use of AgNPs in different templates as a spacer material in SPCE over several years in biochemical research for multifarious applications. Unlike silver, which suffers from quick oxidation and parasitic material Ohmic losses, gold exhibits superior chemical stability and performs excellently in visible and NIR spectral regions. However, gold has not been significantly utilized in different plasmonic nanointerfaces employed in SPCE substrate engineering due to the large unproductive quenching of commonly used fluorescent molecules such as rhodamine dyes encountered with the use of AuNPs. Au is also plagued by huge interband losses in the visible spectrum. MEF primarily depends on the distance between the fluorophores and plasmonic NPs. AuNPs significantly quench the molecular emission from fluorophores (at close distances < 5 nm). To prevent this quenching, several strategies have been employed to provide a spacer layer around the AuNPs to avoid direct contact with fluorophore [37].

Bhaskar et al., have demonstrated a rapid and facile strategy to overcome this limitation by using Au (metal) decorated- SiO_2 (dielectric) NPs (AuSil) [37]. In this study, hybridized AuSil dequenches the otherwise quenched fluorescence emission from radiating dipoles. The comparison of transmission electron microscope (TEM) images of bare SiO_2 NPs (Figure 1a) and synthesized AuSil hybrids (Figure 1b–d) clearly show the decoration of silica surface with gold nanospheres. The lattice fringes with d-spacing of 0.235 and 0.204 Å seen in the high-resolution transmission electron microscope (HRTEM) image of AuSil hybrid (Figure 1d) correspond to the Miller indices (111) and (200) of FCC gold. The particle size distribution histogram along with the percentage distribution for AuNPs and SiO_2 NPs is presented in Figure 1e,f with the average size being 5.7 (± 0.8) nm and 20.3 (± 4.5) nm, respectively [37].

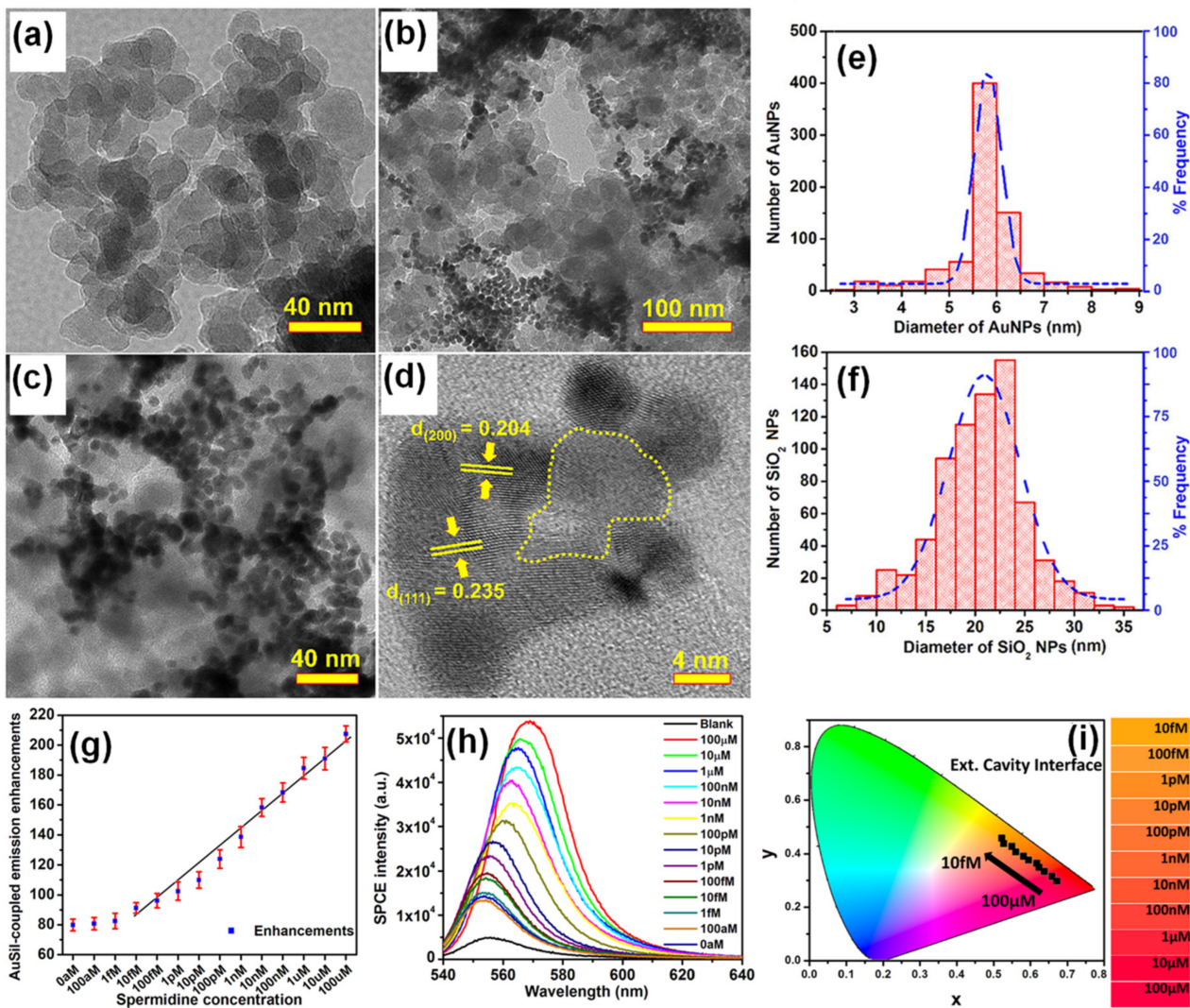


Figure 1. (a) TEM image of SiO₂ NPs. (b-d) TEM images of synthesized Au-decorated SiO₂ (AuSil) nanohybrids at different magnifications. In HRTEM image (d) yellow dotted curve indicates amorphous SiO₂ decorated with crystalline AuNPs (lattice fringes are shown with corresponding Miller indices for gold). (e,f) Particle size distribution histogram of AuNPs and SiO₂ NPs shown along with percentage frequency [right y-axis] obtained from TEM analysis. (g) Plasmon-coupled emission enhancements for increasing concentrations of spermidine taken along with AuSil hybrids in ext. cavity interface. (h) SPCE spectra for corresponding emission enhancements observed in (g). (i) CIE chromaticity plot and corresponding shade card indicating color change in emission pattern consistent with results in (h). Adapted with permission from [37].

The careful choice of nanomaterials used for AuSil hybrid and the appropriate design of extended cavity nanointerface led to an 88-fold enhancement on the SPCE platform. This enhancement obtained with AuSil hybrid increased to 207-fold upon addition of 100 μM concentration of spermidine (Figure 1g), whereas decreasing the concentration of spermidine up to 10 fM allowed for the reliable and sensitive detection of this molecule [37]. The SPCE intensity spectra presenting a clear decrease in emission intensity is in consonance with enhancements (Figure 1h). The work also established a simplistic and reliable sensing platform for the detection of spermidine, a natural polyamine and a significant biomolecule at femtomolar concentration. The modulation in visible color of

emissions from fluorescent molecules was captured using the smartphone camera, processed using the color grab Android app, and presented in a CIE chromaticity diagram (**Figure 1i**) along with their respective shade card portion on its right [37]. One can clearly notice a hypsochromic shift in the emission profile of fluorescent molecules as the concentration of spermidine is decreased. Modulation of the local density of states of fluorophores were observed by loading AuNPs on SiO_2 NPs at different concentrations and studied in spacer, cavity and extended cavity nanointerfaces. The multi-fold hot-spots rendered by the AuSil nanohybrids assisted in the augmentation of emission radiation which was captured using a smartphone-based SPCE platform, presenting an excellent reliability and reproducibility as a detection system. Quench-free AuSil nanohybrids opens a new vista of exploration in other polaritonic systems such as photonic crystals, silicon, and graphene plasmonics.

4. Effect of Sharp-Edged AuNPs in SPCE

LSPR field enhancement effects of noble metallic NPs can be exploited to enhance the performance of diverse luminescent materials and devices, in which the spectral proximity plays an important role in increasing near-field enhancement-induced excitation (NFEE) and SPCE efficiencies. In their work, Wang et al., have simultaneously utilized the transversal and longitudinal SPR bands of elongated gold nanocrystals to match with the excitation and emission wavelengths of emitters, respectively, to achieve the most efficient enhancement in Polymer light-emitting diodes (PLEDs), which are the next-generation flat-panel display platforms [38].

Four types of gold nanomaterials as shown in **Figure 2a–d** (AuNPs, diameter = 20 nm), gold nanorods (AuNRs, length/width = 80/40 nm; 90/30 nm), and gold nano-bipyramids (AuNBPs, length/width = 80/40 nm) were employed as the plasmonic nanoantennas, according to spectral characteristics of the chosen emitter poly(2-methoxy-5-(2'-ethyl-hexoxy)-1,4-phenylenevinylene) (MEH-PPV). It was experimentally observed that AuNPs (20 nm), AuNRs (80/40 nm), AuNBPs (80/40 nm), and AuNRs (90/30 nm) demonstrated 1.5, 2.1, 2.3, and 1.2 times enhancement in luminance and 1.4, 1.9, 2.0, and 1.1 times enhancement in luminous efficiency in comparison with the pristine device, respectively [38]. Due to the double SPR bands of both AuNBPs (80/40 nm) and AuNRs (80/40 nm) overlapping well with the excitation and emission wavelengths of MEH-PPV, a maximum 2.2- and 2.1-times enhancement in photoluminescence intensity was observed, respectively. By controlling the aspect ratios of Gold nanorods (AuNRs) and gold nano-bipyramids (AuNBPs), tunability of their longitudinal SPR bands could be achieved. The device structure of plasmon-mediated PLEDs adopted ITO/nanometals/ZnO/MEH-PPV/MoO₃/Ag is displayed in **Figure 2e**. The average distance between the emitter and plasmonic nanometals was controlled in the range 10–15 nm. A representative energy level diagram of the device is additionally depicted in **Figure 2f**. Because the electron mobility of MEH-PPV is about three orders of magnitude smaller than the hole mobility, the excitons derived from hole/electron recombination are mainly formed near the ZnO/MEH-PPV interface [38]. Thus, the EM field of nanometals can effectively promote the excitons transferring to emitting photons. The performance of the pristine device and hybrid ones with different morphologies and optimized amounts of Au nanocrystals are shown in **Figure 2c,d**.

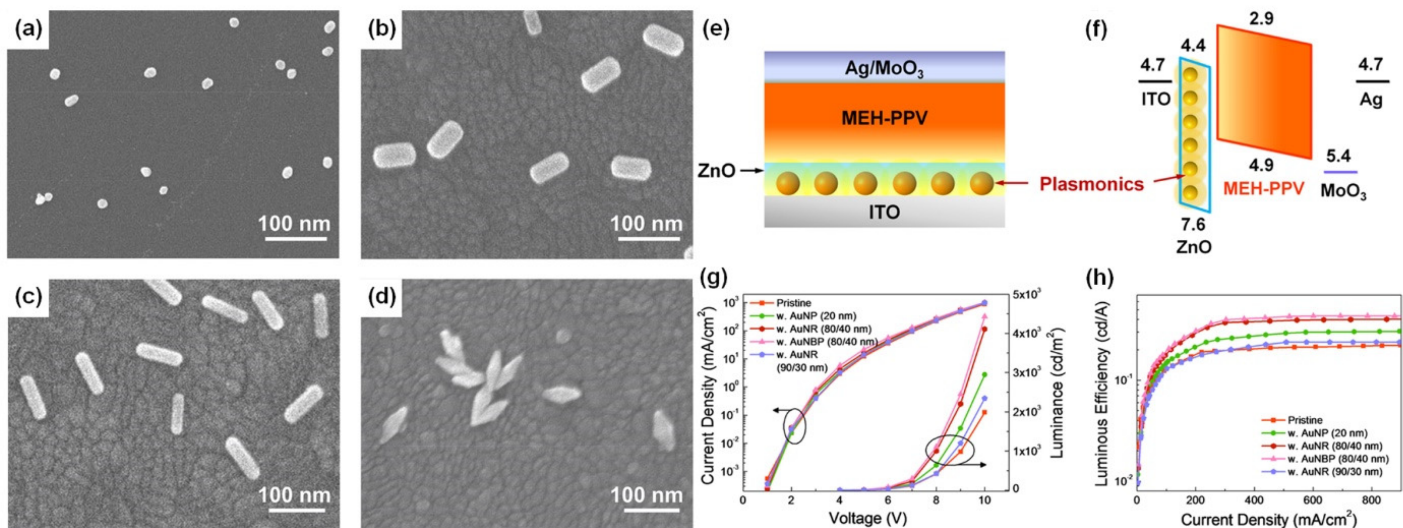


Figure 2. SEM images of (a) AuNPs (20 nm), (b,c) AuNRs (80/40 nm, 90/30 nm), and (d) AuNPs (80/40 nm) deposited on the ITO substrate by the electrostatic adsorption, (e) schematic layout of plasmon-mediated PLEDs. (f) Energy level diagrams of ITO, ZnO, MEH-PPV, MoO₃, and Ag. PLED characteristics of (g) current density vs applied voltage (J–V) and luminance vs applied voltage (L–V), and (h) luminous efficiency vs. current density (LE–J) curves, including pristine and hybrid devices with different morphologies and optimized amounts of Au nanocrystals. Adapted with permission from [38].

Compared to AuNRs, AuNPs are highly monodisperse, which suppresses the inhomogeneous spectral broadening for the plasmon peaks and the local electric field enhancements of AuNPs are several times larger than those of AuNRs [38]. The integration of the NFEE and SPCE effects of AuNRs and AuNPs derived from their double SPR modes, leads to simultaneous excitation and emission enhancements as made evident by steady-state and time-resolved PL measurements. This study not only systematically explores LSPL field enhancement effects of size and shape-controlled Au nanocrystals on the PLEDs' performance but also demonstrates that AuNPs can be applied in electroluminescence devices to enhance the emission intensity and efficiency.

Dissipative Ohmic losses due to electron scattering at the lattice of AuNPs leads to predominant non-radiative decay and quenching of fluorophores. While the incident light scatters, the lattice vibrations within the crystal lattice results in dissipative heat losses through absorption. Hence, the scattering and absorption (extinction) reduces the intensity of incident EM-field. The enhanced quenching of fluorophore with a distance < 5 nm from AuNPs is a fundamental caveat for exploiting the utility of AuNPs in SPCE. In order to address this limitation, AuNPs with nanostructures that can overcome quenching and yield multifold hot-spots with EM-field confinement need to be deployed to enhance the luminescence signal intensity [39].

The appropriate choice of metal thin films (Ag, Au, Cu and Pt) and NPs with desired shape, size, and aspect ratios in suitable nano-environment can mitigate the limitations of quenching. In comparison to Ag, Al, Cu and alkali metals, Au exhibits greater chemical stability with excellent performance in visible and near-infrared (NIR) spectral regions [39]. Apart from being biocompatible, its diverse surface functionalities have rendered Au, suitable for

biomedical applications. NPs with sharp edges, crevices, tips and voids are known to entrap the incident light energy to subwavelength regions. Although the 'lightning rod effect' supported by nanorods exceptionally enhances the local electric-field, morphologically similar effects can be obtained from nanostars (NSs) [40].

Chandran and co-workers have demonstrated the robustness of gold nanostars (AuNSs) to simultaneously obtain template-free dequenched, enhanced (100-fold), highly polarized and directional emission in SPCE [39]. The overall dipole moment of the tip plasmons is maximized on account of coupling between the tip and core plasmons which in turn amplifies EM-field intensity in their vicinity. The sharp edges with vortices in AuNSs supporting enhanced electronic cloud perturbations that couple with nearby fluorophores, overcome the competing quenching phenomenon observed with spherical AuNPs to a large extent. **Figure 3a** shows SPR characteristic of AuNPs in the visible region of λ_{max} : 530 nm. **Figure 3b** shows the SPR band of AuNSs with a λ_{max} : 670 nm. The TEM image shown in **Figure 3c** presents gold nanospheres that are uniform in size with an average size of 16 ± 2 nm. HRTEM imaging further confirms the formation of polycrystalline AuNPs: lattice fringes observed with d-spacings of 2.36 Å and 2.05 Å correspond to the (111) and (200) Bragg planes of FCC gold. HRTEM images in **Figure 3d,e** also clearly reveal the star-shaped morphology of the reduced gold (AuNSs) [39]. Lattice fringes, as seen in the HRTEM image (**Figure 3f**) of a sharp arm of one of the AuNSs clearly reveals d-spacing corresponding to (200) Bragg planes of FCC gold (2.03 Å), and confirms the formation of AuNSs. **Figure 3g** shows that enhancements increased to 100, 88 and 76-fold in spacer, cavity and ext. cavity interfaces, respectively. The decline in emissions for the ext. cavity is on account of scattering of the incident beam by sharp edges and vortices of AuNSs [39]. The increase in SPCE signal intensity with the use of AuNSs in comparison to blank and FS emission is presented in **Figure 3h** along with corresponding angularity plot showing high directionality in **Figure 3i**. Electrodynamic calculations such as discrete dipole approximation (DDA) have shown that regions in plasmonic materials having sharp tips have enhancements several orders of magnitude as compared with incident field. This approach for realizing dequenched and augmented emissions using gold NPs without the additional templates will help realize novel approach for point-of-care diagnostics.

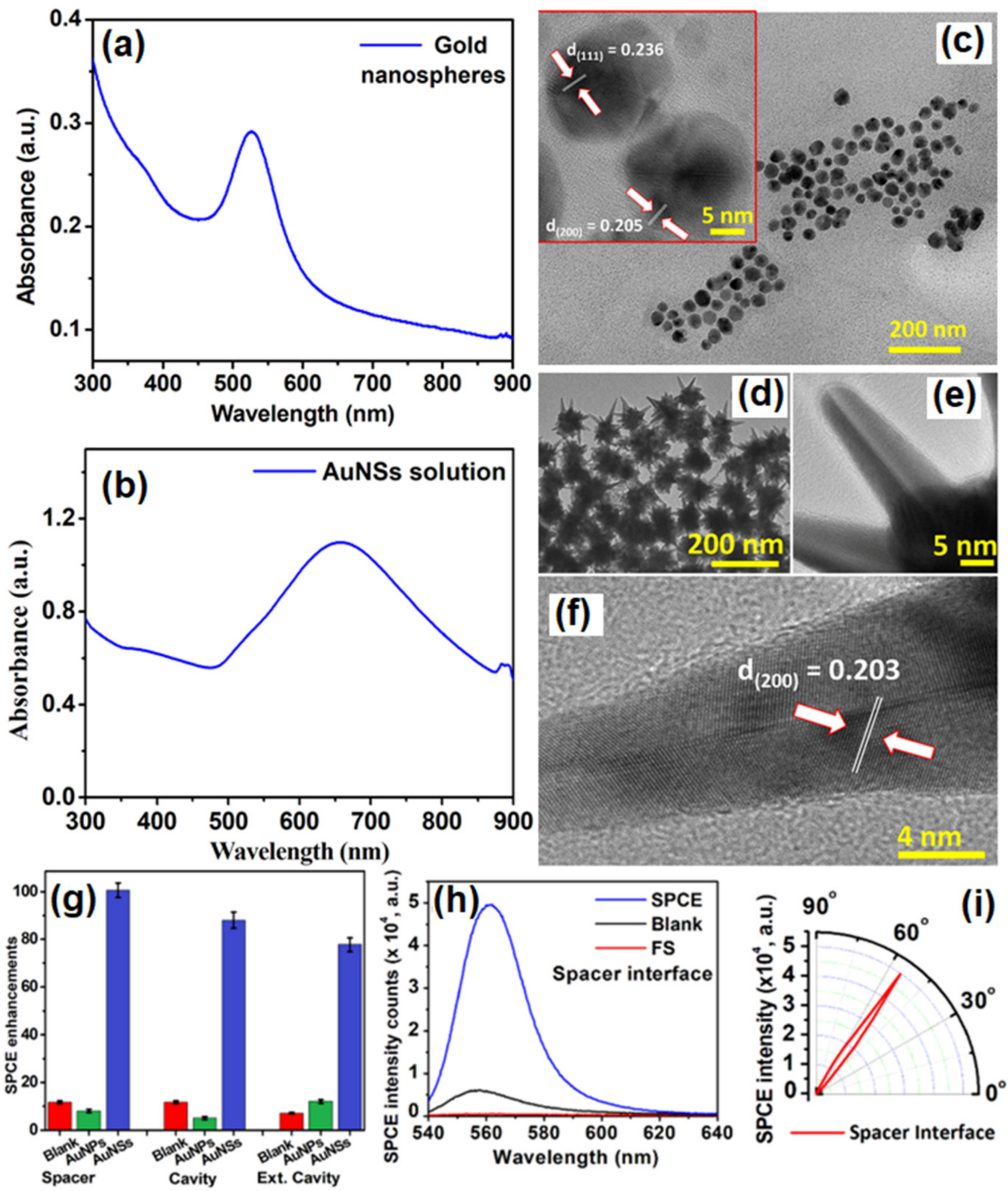


Figure 3. (a) UV-vis absorbance profile of AuNPs (b) UV-Vis absorbance profile of AuNSs. (c) TEM image of synthesized AuNPs and HRTEM image of AuNPs indicating the lattice fringes characteristic to gold (inset). (d,e): TEM images of synthesized AuNSs. (f) HRTEM image of AuNSs indicating the lattice fringes along with d-spacing and Miller indices characteristic of gold. (g) Comparative assessment of SPCE emission enhancements for AuNPs and AuNSs along with respective blanks in spacer, cavity and ext. cavity interfaces. (h) SPCE and FS emission

intensity obtained with AuNSs along with blank in spacer interface. (i) Angularity plot for SPCE with AuNSs in spacer interface. (h,i) are chosen for representation because spacer interface presented maximum emission enhancements. Adapted with permission from [39].

5. Effect of Hollow AuNPs in SPCE

The use of solid NPs in SPCE-based sensing has gradually expanded to hollow NPs owing to their numerous advantages. The LSPR peaks of hollow NPs can be easily shifted from the visible region to the near-IR region by changing the dimensions of the NP core and shell. The plasmon of the hollow NP exhibits a large spectral shift as a result of the change in the refractive index in their immediate vicinity, which consequently improves their sensing capability. The EM field of the hollow NP is strong, which is attributed to the intense plasmonic coupling between the inner and outer surfaces.

Xie et al. have reported that by assembling GNSs on a gold substrate via electrostatic adsorption and subsequently applying a fluorophore layer by spin-coating, SPCE fluorescence signals exhibited 30- and 110-fold enhancements compared to those of normal SPCE and free space emissions, respectively [41]. After the junction of GNSs on a gold substrate, a “hot-spot” structure emerged between the gold substrate and GNS because of the interaction between the localized and propagating SPs. This produced a more intense EM field; specifically, the EM field around the “hot-spot” was twice as strong as that around the GNS, which was confirmed by comparing the scale bars in **Figure 4a,b**.

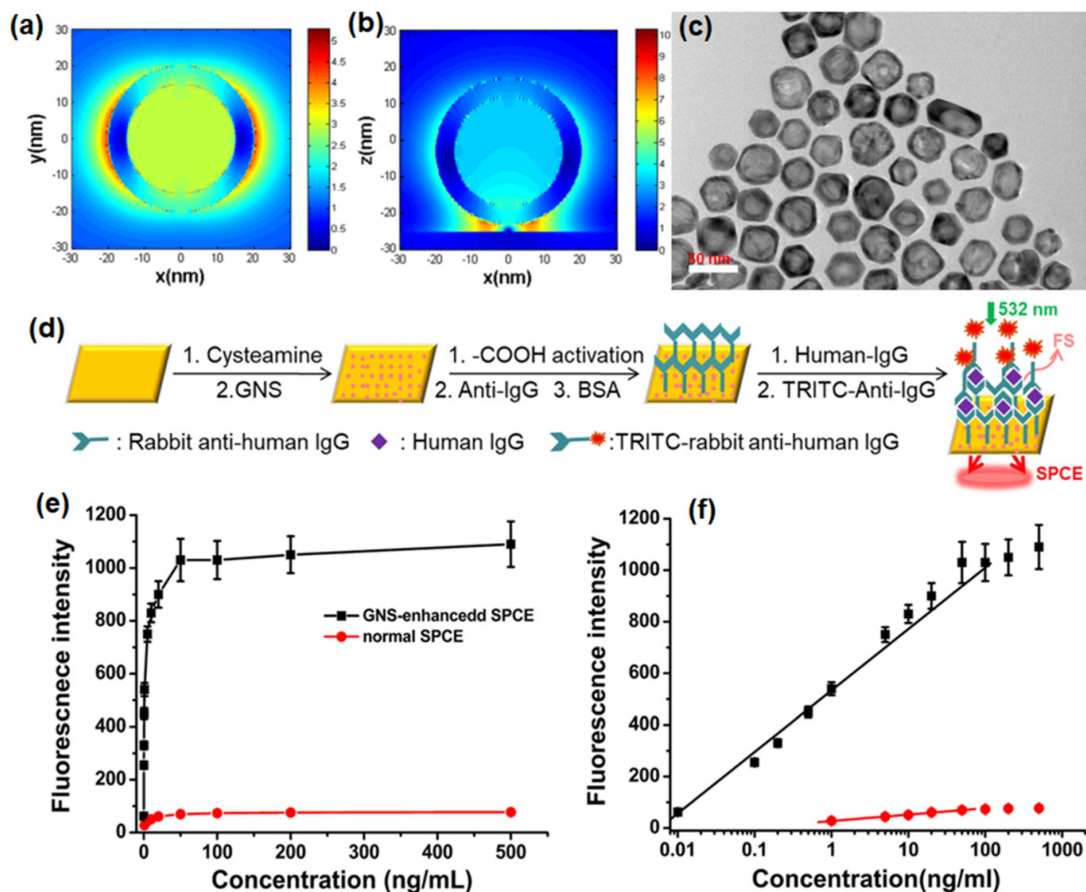


Figure 4. Finite-difference time-domain (FDTD) simulations for the near field region of (a) a single GNS (diameter: 40 nm; shell thickness: 5 nm) and (b) a gold substrate modified with GNS at 532 nm (diameter: 40 nm; shell thickness: 5 nm; distance between GNS and gold substrate: 2 nm; thickness of gold substrate: 50 nm). (c) TEM image of GNS displayed the desired hollow structures coated with a thick gold layer. (d) The sensing schematic diagram (this diagram is not to scale). (e) Fluorescence intensities for immunosensors based on GNS-enhanced SPCE (black) and normal SPCE (red). (f) Dependence of the fluorescence intensity of GNS-enhanced SPCE (black) and normal SPCE (red) on the concentration of human IgG. The fluorophores employed were TRITC. Adapted with permission from [41].

The TEM images of GNS hollow structures with a diameter of approximately 30 nm are seen in **Figure 4c**. An SPCE-based biosensor comprising GNSs assembled on a gold substrate could detect proteins (human IgG) via an established immuno-sandwich structure on the modified substrate surface (**Figure 4d**) [41]. The signal was observed to increase with increasing concentration of human IgG and the immunoassay results for both the normal SPCE and GNS enhanced SPCE systems is shown in **Figure 4e**. Moreover, a linear relationship ($R = 0.994$) was noted between the GNS-enhanced SPCE signal and the antigen concentration over a concentration range of 0.01 to 100 ng/mL with a detection limit of 0.004 ng/mL. In contrast, the linearity range for normal SPCE (**Figure 4f**) was only observed over a concentration range of 1 to 50 ng/mL with a detection limit of 0.2 ng/mL. Therefore, introducing GNSs provided the SPCE system with a higher detection sensitivity, a wider detection range, and a much lower detection limit [41].

Hence, it has been demonstrated that the GNS-enhanced SPCE system was suitable for biomolecule detection because of the scale match between the optimal fluorophore thickness and the biomolecule size, and thus was designed as an immunosensor to verify the feasibility of this system. This GNS-enhanced SPCE system provides several advantages. There is considerable signal enhancement due to the hollow plasmonic NPs without complex modifications or redundant, assistive materials, which greatly simplified the enhancing strategy. This method works effectively under a defined layer thickness (approximately 30 nm), which is very suitable for biomolecule detection and imaging. An appropriate GNS size helps to position the fluorophores in the effective coupling zone, which can provide enhanced signal with higher stability [41]. This strategy of introducing GNSs in SPCE has created a new fluorescence system based on a hollow plasmonic structure and provides a simple way to improve the detection sensitivity in fluorescence-based sensing and imaging platforms.

In another approach, Xie and co-workers utilized the gold nanocages (AuNCs) to generate high field confinement and fluorescence enhancement with factors over 150 and 600 compared with the normal SPCE and free space emission [42]. This is accomplished by using a thin 10 nm fluorophore layer over the SPCE substrate, thereby presenting an effective approach to dequench the otherwise quenched emission induced by resonance energy transfer (in normal SPCE) signal. The TEM characterization of the AuNCs is presented in **Figure 5a** along with the size distribution in **Figure 5b**. Recently, different simulation tools such as FDTD, COMSOL Multiphysics, DDA to name a few have been used to evaluate the EM hotspot intensity in the nanogaps generated by the plasmonic nanomaterials [42]. The FDTD simulations (based on Lumerical Solutions) were adopted to understand the near-field EM field patterns of a single AuNC with and without the gold substrate.

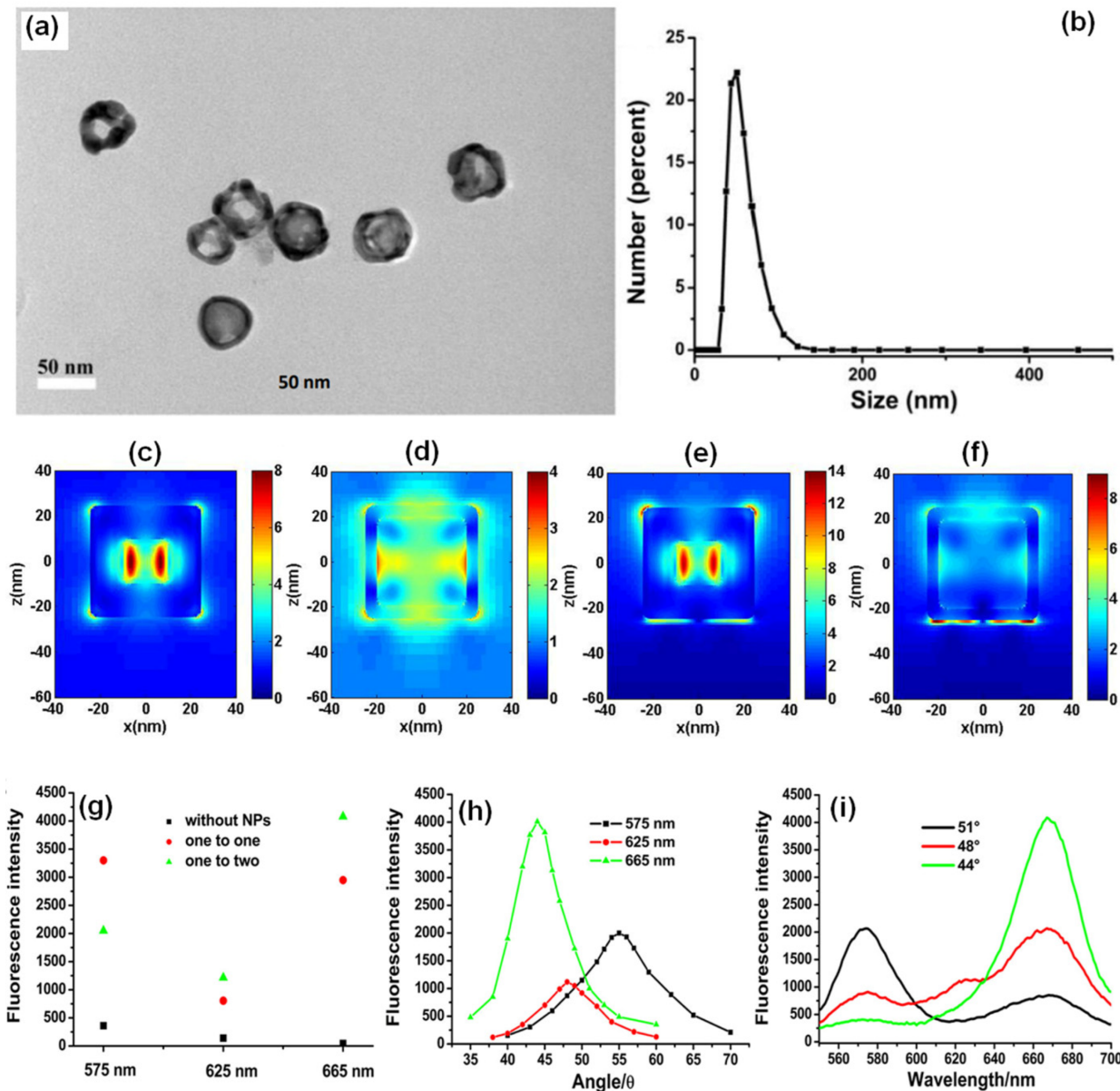


Figure 5. (a) The TEM images and (b) the DLS size distribution of AuNCs. FDTD simulation results of the near-field of a single AuNC and gold substrate with the AuNC at 532 nm (c,e): the outside surface; (d,f): the inside of the AuNC). Length of AuNC: 50 nm; length of hole: 20 nm; shell thickness: 5 nm; distance between AuNC and gold substrate: 2 nm; thickness of gold substrate: 50 nm. (g) SPCE signals of different wavelengths for different mixed ratios, (h) angle distributions for different emission wavelengths, and (i) the fluorescence spectra obtained from different optimal emission angles for different wavelengths (mixed ratio was one to two for GNSs to AuNCs). Adapted with permission from [42].

From **Figure 5c–f**, a significant enhancement in the field intensity is observed not only on the outside of the shell, but also on the interior nano-gap based hotspot. Such coupling of fields from both the plasmonic hotspots within and outside the nanoshell is expected to yield dramatically high fluorescence enhancements due to the mixing or hybridization of modes resulting in higher local density of states [42]. The high field enhancement thus obtained was used by the authors to further utilize the same for development of multiwavelength detection system. This was

accomplished by using GNSs and AuNCs that were mixed with quantum dots solution. It was observed that without the incorporation of the NPs in to the QDs solution, the multiwavelength detection system was not effective [42]. However, upon mixing the plasmonic NPs of different aspect ratios (shells and cubes) the emission intensity at all the desired wavelengths were enhanced. That is, with the incorporation of NPs the signals which were otherwise non-detectable were identified with the addition of plasmonic gold nanoparticles (**Figure 5g–i**). These results present the gold-based nano-engineering with hollow structures and different aspect ratios to be ideal candidates to accomplish multiwavelength simultaneous fluorescence enhancement and detection facilitating multi-analyte sensing as well as associated imaging [42].

References

1. Badshah, M.A.; Koh, N.Y.; Zia, A.W.; Abbas, N.; Zahra, Z.; Saleem, M.W. Recent Developments in Plasmonic Nanostructures for Metal Enhanced Fluorescence-Based Biosensing. *Nanomaterials* 2020, 10, 1749.
2. Bauch, M.; Toma, K.; Toma, M.; Zhang, Q.; Dostalek, J. Plasmon-Enhanced Fluorescence Biosensors: A Review. *Plasmonics* 2014, 9, 781–799.
3. Cao, S.-H.; Cai, W.-P.; Liu, Q.; Li, Y.-Q. Surface Plasmon–Coupled Emission: What Can Directional Fluorescence Bring to the Analytical Sciences? *Annu. Rev. Anal. Chem.* 2012, 5, 317–336.
4. Lakowicz, J.R. Radiative Decay Engineering 5: Metal-Enhanced Fluorescence and Plasmon Emission. *Anal. Biochem.* 2005, 337, 171–194.
5. Zhang, C.; Qi, J.; Li, Y.; Han, Q.; Gao, W.; Wang, Y.; Dong, J. Surface-plasmon-assisted growth, reshaping and transformation of nanomaterials. *Nanomaterials* 2022, 12, 1329.
6. Mi, X.; Zhang, T.; Zhang, C.; Wang, Y.; Chen, H.; Li, J.; Fu, Z.; Zhang, Z.; Zheng, H. Plasmonic sensing of Cu²⁺ via shell-etching of Au@ Ag nanorods. *Mater. Chem. Phys.* 2021, 259, 124036.
7. Taylor, A.B.; Zijlstra, P. Single-Molecule Plasmon Sensing: Current Status and Future Prospects. *ACS Sens.* 2017, 2, 1103–1122.
8. Jabbar, A.; Abbas, A.; Assad, N.; Naeem-ul-Hassan, M.; Alhazmi, H.A.; Najmi, A.; Zoghebi, K.; Bratty, M.A.; Hanbashi, A.; Amin, H.M.A. A Highly Selective Hg²⁺ Colorimetric Sensor and Antimicrobial Agent Based on Green Synthesized Silver Nanoparticles Using *Equisetum Diffusum* Extract. *RSC Adv.* 2023, 13, 28666–28675.
9. Hamza, M.E.; Othman, M.A.; Swillam, M.A. Plasmonic Biosensors: Review. *Biology* 2022, 11, 621.

10. Pruchyathamkorn, J.; Yang, M.; Amin, H.M.A.; Batchelor-McAuley, C.; Compton, R.G. Imaging Electrode Heterogeneity Using Chemically Confined Fluorescence Electrochemical Microscopy. *J. Phys. Chem. Lett.* 2017, 8, 6124–6127.
11. Thacharakkal, D.; Bhaskar, S.; Sharma, T.; Rajaraman, G.; Sathish Ramamurthy, S.; Subramaniam, C. Plasmonic Synergism in Tailored Metal–Carbon Interfaces for Real-Time Single Molecular Level Sniffing of PFOS and PFOA. *Chem. Eng. J.* 2023, 480, 148166.
12. Dai, P.; Li, H.; Huang, X.; Wang, N.; Zhu, L. Highly sensitive and stable copper-based SERS chips prepared by a chemical reduction method. *Nanomaterials* 2021, 11, 2770.
13. Mejía-Salazar, J.R.; Oliveira, O.N., Jr. Plasmonic Biosensing. *Chem. Rev.* 2018, 118, 10617–10625.
14. Cai, R.; Yin, L.; Huang, Q.; You, R.; Feng, S.; Lu, Y. An endoscope-like sers probe based on the focusing effect of silica nanospheres for tyrosine and urea detection in sweat. *Nanomaterials* 2022, 12, 421.
15. Liu, J.; Jalali, M.; Mahshid, S.; Wachsmann-Hogiu, S. Are Plasmonic Optical Biosensors Ready for Use in Point-of-Need Applications? *Analyst* 2020, 145, 364–384.
16. Arathi, P.J.; Seemesh, B.; Ramanathan, V. Disulphide Linkage: To Get Cleaved or Not? Bulk and Nano Copper Based SERS of Cystine. *Spectrochim. Acta Part A Mol. Biomol. Spectrosc.* 2018, 196, 229–232.
17. Shrivastav, A.M.; Cvelbar, U.; Abdulhalim, I. A Comprehensive Review on Plasmonic-Based Biosensors Used in Viral Diagnostics. *Commun. Biol.* 2021, 4, 70.
18. Minopoli, A.; Acunzo, A.; Della Ventura, B.; Velotta, R. Nanostructured Surfaces as Plasmonic Biosensors: A Review. *Adv. Mater. Interfaces* 2022, 9, 2101133.
19. Utility of Nanotechnology in Dye Degradation. Available online: <http://benthamscience.com/chapter/21154> (accessed on 21 December 2023).
20. Borisov, S.M.; Wolfbeis, O.S. Optical Biosensors. *Chem. Rev.* 2008, 108, 423–461.
21. Burda, C.; Chen, X.; Narayanan, R.; El-Sayed, M.A. Chemistry and Properties of Nanocrystals of Different Shapes. *Chem. Rev.* 2005, 105, 1025–1102.
22. Bhaskar, S. Biosensing Technologies: A Focus Review on Recent Advancements in Surface Plasmon Coupled Emission. *Micromachines* 2023, 14, 574.
23. Rai, A.; Bhaskar, S.; Ganesh, K.M.; Ramamurthy, S.S. Hottest Hotspots from the Coldest Cold: Welcome to Nano 4.0. *ACS Appl. Nano Mater.* 2022, 5, 12245–12264.
24. Lakowicz, J.R.; Ray, K.; Chowdhury, M.; Szmacinski, H.; Fu, Y.; Zhang, J.; Nowaczyk, K. Plasmon-Controlled Fluorescence: A New Paradigm in Fluorescence Spectroscopy. *Analyst* 2008,

133, 1308–1346.

25. Rai, A.; Bhaskar, S.; Reddy, N.; Ramamurthy, S.S. Cellphone-Aided Attomolar Zinc Ion Detection Using Silkworm Protein-Based Nanointerface Engineering in a Plasmon-Coupled Dequenched Emission Platform. *ACS Sustain. Chem. Eng.* 2021, 9, 14959–14974.

26. Chen, X.; Xu, W.; Zhu, Y.; Zhou, P.; Cui, S.; Tao, L.; Xu, L.; Song, H. Nd₂O₃/Au nanocomposites: Upconversion broadband emission and enhancement under near-infrared light excitation. *J. Mater. Chem. C* 2014, 2, 5857–5863.

27. Lis S, S.M.; Bhaskar, S.; Dahiwadkar, R.; Kanvah, S.; Ramamurthy, S.S.; Bhaktha B. N., S. Plasmon-Rich BCZT Nanoparticles in the Photonic Crystal-Coupled Emission Platform for Cavity Hotspot-Driven Attomolar Sensing. *ACS Appl. Nano Mater.* 2023, 6, 19312–19326.

28. Rai, A.; Bhaskar, S.; Mohan, G.K.; Ramamurthy, S.S. Biocompatible Gellucire® Inspired Bimetallic Nanohybrids for Augmented Fluorescence Emission Based on Graphene Oxide Interfacial Plasmonic Architectures. *ECS Trans.* 2022, 107, 4527.

29. Lv, J.; Liang, T.; Gu, Q.; Liu, Q.; Ying, Y.; Si, G. A High Refractive Index Plasmonic Micro-Channel Sensor Based on Photonic Crystal Fiber. *Nanomaterials* 2022, 12, 3764.

30. Bhaskar, S.; Sathish Ramamurthy, S. Performance Enhancement of Light Emitting Radiating Dipoles (LERDs) Using Surface Plasmon-Coupled and Photonic Crystal-Coupled Emission Platforms. In *Organic and Inorganic Light Emitting Diodes: Reliability Issues and Performance Enhancement*; CRC Press: Boca Raton, FL, USA, 2023; pp. 161–184.

31. Rai, A.; Bhaskar, S.; Ramamurthy, S.S. Plasmon-Coupled Directional Emission from Soluplus-Mediated AgAu Nanoparticles for Attomolar Sensing Using a Smartphone. *ACS Appl. Nano Mater.* 2021, 4, 5940–5953.

32. da Silva, R.T.; de Souza Rodrigues, M.P.; Davilla, G.F.; da Silva, A.M.; Dourado, A.H.; Córdoba de Torresi, S.I. AgAu hollow nanoshells on layered graphene oxide and silica submicrospheres as plasmonic nanozymes for light-enhanced electrochemical H₂O₂ sensing. *ACS Appl. Nano Mater.* 2021, 4, 12062–12072.

33. Cao, S.-H.; Weng, Y.-H.; Xie, K.-X.; Wang, Z.-C.; Pan, X.-H.; Chen, M.; Zhai, Y.-Y.; Xu, L.-T.; Li, Y.-Q. Surface Plasmon Coupled Fluorescence-Enhanced Interfacial “Molecular Beacon” To Probe Biorecognition Switching: An Efficient, Versatile, and Facile Signaling Biochip. *ACS Appl. Bio Mater.* 2019, 2, 625–629.

34. Weng, Y.-H.; Xu, L.-T.; Chen, M.; Zhai, Y.-Y.; Zhao, Y.; Ghorai, S.K.; Pan, X.-H.; Cao, S.-H.; Li, Y.-Q. In Situ Monitoring of Fluorescent Polymer Brushes by Angle-Scanning Based Surface Plasmon Coupled Emission. *ACS Macro Lett.* 2019, 8, 223–227.

35. Erdogan, K.; Yucel, O.; Oruc, M.E. Investigation of Structural, Morphological, and Optical Properties of Novel Electrospun Mg-Doped TiO₂ Nanofibers as an Electron Transport Material for

Perovskite Solar Cells. *Nanomaterials* 2023, 13, 2255.

36. Xie, K.-X.; Liu, C.; Liu, Q.; Xiao, X.-X.; Li, Z.; Li, M.-F. Multiarchitecture-Based Plasmonic-Coupled Emission Employing Gold Nanoparticles: An Efficient Fluorescence Modulation and Biosensing Platform. *Langmuir* 2021, 37, 11880–11886.

37. Bhaskar, S.; Kowshik, N.C.S.S.; Chandran, S.P.; Ramamurthy, S.S. Femtomolar Detection of Spermidine Using Au Decorated SiO₂ Nanohybrid on Plasmon-Coupled Extended Cavity Nanointerface: A Smartphone-Based Fluorescence Dequenching Approach. *Langmuir* 2020, 36, 2865–2876.

38. Wang, H.; Zhang, B.; Zhao, Y.; Chen, X.; Zhang, Z.; Song, H. Integrated Effects of Near-Field Enhancement-Induced Excitation and Surface Plasmon-Coupled Emission of Elongated Gold Nanocrystals on Fluorescence Enhancement and the Applications in PLEDs. *ACS Appl. Electron. Mater.* 2019, 1, 2116–2123.

39. Bhaskar, S.; Patra, R.; Kowshik, N.C.S.S.; Ganesh, K.M.; Srinivasan, V.; Chandran S, P.; Ramamurthy, S.S. Nanostructure Effect on Quenching and Dequenching of Quantum Emitters on Surface Plasmon-Coupled Interface: A Comparative Analysis Using Gold Nanospheres and Nanostars. *Phys. E Low-Dimens. Syst. Nanostruct.* 2020, 124, 114276.

40. Fukuoka, N.; Tanabe, K. Lightning-Rod Effect of Plasmonic Field Enhancement on Hydrogen-Absorbing Transition Metals. *Nanomaterials* 2019, 9, 1235.

41. Xie, K.-X.; Liu, Q.; Jia, S.-S.; Xiao, X.-X. Fluorescence Enhancement by Hollow Plasmonic Assembly and Its Biosensing Application. *Anal. Chim. Acta* 2021, 1144, 96–101.

42. Xie, K.-X.; Liu, Q.; Song, X.-L.; Huo, R.-P.; Shi, X.-H.; Liu, Q.-L. Amplified Fluorescence by Hollow-Porous Plasmonic Assembly: A New Observation and Its Application in Multiwavelength Simultaneous Detection. *Anal. Chem.* 2021, 93, 3671–3676.

Retrieved from <https://encyclopedia.pub/entry/history/show/121863>